

# A Short Mitochondrial Form of p19<sup>ARF</sup> Induces Autophagy and Caspase-Independent Cell Death

Sharon Reef,<sup>1</sup> Einat Zalckvar,<sup>1</sup> Ohad Shifman,<sup>2</sup> Shani Bialik,<sup>1</sup> Helena Sabanay,<sup>3</sup> Moshe Oren,<sup>2</sup> and Adi Kimchi<sup>1,\*</sup>

<sup>1</sup>Department of Molecular Genetics

<sup>2</sup>Department of Molecular Cell Biology

<sup>3</sup>Chemical Research Support

Weizmann Institute of Science

Rehovot 76100

Israel

## Summary

The tumor suppressor functions of p19<sup>ARF</sup> have been attributed to its ability to induce cell cycle arrest or apoptosis by activating p53 and regulating ribosome biogenesis. Here we describe another cellular function of p19<sup>ARF</sup>, involving a short isoform (smARF, short mitochondrial ARF) that localizes to a Proteinase K-resistant compartment of the mitochondria. smARF is a product of internal initiation of translation at Met45, which lacks the nucleolar functional domains. The human p14<sup>ARF</sup> mRNA likewise produces a shorter isoform. smARF is maintained at low levels via proteasome-mediated degradation, but it increases in response to viral and cellular oncogenes. Ectopic expression of smARF reduces mitochondrial membrane potential ( $\Delta\Psi_m$ ) without causing cytochrome c release or caspase activation. The dissipation of  $\Delta\Psi_m$  does not depend on p53 or Bcl-2 family members. smARF induces massive autophagy and caspase-independent cell death that can be partially rescued by knocking down ATG5 or Beclin-1, suggesting a different prodeath function for this short isoform.

## Introduction

The ARF tumor suppressor protein (p19<sup>ARF</sup> in mouse and p14<sup>ARF</sup> in human) is an activator of p53 that antagonizes the function of p53's inhibitor, Mdm2. ARF inhibits Mdm2 by sequestering it to the nucleolus (Tao and Levine, 1999; Weber et al., 1999) and by inhibiting its E3 protein ubiquitin ligase activity (Honda and Yasuda, 1999; Midgley et al., 2000). ARF is induced by oncoproteins such as c-Myc (Zindy et al., 1998), E2F-1 (Bates et al., 1998), and  $\beta$ -catenin (Damalas et al., 2001) and is thus an important mediator in the activation of p53 in response to oncogenes (Lowe and Sherr, 2003). Yet, the seminal finding that mice lacking p19<sup>ARF</sup>, p53, and Mdm2 are more tumor prone than those lacking only p53 and Mdm2 raised the possibility that p19<sup>ARF</sup> can also act independently of the Mdm2-p53 axis in tumor surveillance (Weber et al., 2000a). Consistent with this notion, studies performed in cell culture have shown that the two cellular effects of p19<sup>ARF</sup>, i.e., inhibition of cell growth/proliferation and induction of apoptosis, can also occur in a p53-Mdm2-independent manner (Matsuoka et al., 2003; Nakazawa et al., 2003; Sugimoto

et al., 2003; Suzuki et al., 2003; Tsuji et al., 2002). The inhibitory functions on cellular growth have been associated with inhibition of rRNA processing in the nucleolus via physical interactions with nucleophosmin/B23 (Bertwistle et al., 2004; Sugimoto et al., 2003). Yet, p53-independent molecular mechanisms mediating the prodeath mode of action of p19<sup>ARF</sup> have not been thoroughly determined.

The murine p19<sup>ARF</sup> is composed of 169 amino acids, is highly basic and hydrophobic, and localizes primarily to nucleoli (Weber et al., 1999). The human p14<sup>ARF</sup> ortholog is composed of only 132 amino acids and shares only limited sequence homology with the mouse protein (Stott et al., 1998). Yet, p14<sup>ARF</sup> is also a basic and hydrophobic protein that often localizes predominantly to the nucleolus (Lohrum et al., 2000), and it retains all known tumor suppressor functions of the mouse p19<sup>ARF</sup> protein as well as p19<sup>ARF</sup>'s capability to induce p53-independent apoptosis (Hemmati et al., 2002).

Here we report on a mitochondrial short form of p19<sup>ARF</sup>, designated smARF (short mitochondrial ARF), which results from internal initiation of translation. smARF causes dissipation of mitochondrial membrane potential ( $\Delta\Psi_m$ ), in a p53- and Bcl-2-family-independent manner, without releasing cytochrome c. It leads to the induction of massive autophagy and to caspase-independent cell death. Notably, although the mouse and the human ARF mRNA share only limited sequence homology, the ability to produce a shorter protein form is preserved between the orthologs, emphasizing the importance of this ARF isoform.

## Results

### Internal Initiation of Translation Generates a Short Form of p19<sup>ARF</sup>

The murine p19<sup>ARF</sup> is composed of 169 amino acids (Figure 1A). In addition to the full-length protein, ectopic expression of p19<sup>ARF</sup>-Flag cDNA in 293T cells gave rise to a shorter, faster migrating form, which we designated smARF (Figure 1B). The levels of smARF corresponded to about 1%–5% of total p19<sup>ARF</sup> protein. It should be noted that this form was detected only under gel conditions that efficiently resolved low-molecular-weight proteins, which may explain why smARF has not been previously reported. smARF was detected by Western blotting with either anti-Flag or anti-p19<sup>ARF</sup> antibodies (Figures 1B and 1C), indicating that smARF contains an intact C terminus. It was also present when cells were directly lysed in sample loading buffer (Figure 1C), excluding the possibility that smARF is a degradation product generated during the extraction procedure.

One mechanism that may account for the formation of smARF is translation from an internal initiation site. In fact, the p19<sup>ARF</sup> mRNA sequence contains a single additional Met at position 45 (Figure 1A), which potentially could function as an internal initiation site. Expression of a plasmid in which Met1 was converted to Ile (p19<sup>ARF</sup> M1I) resulted in abundant production of a protein product whose electrophoretic mobility was

\*Correspondence: adi.kimchi@weizmann.ac.il

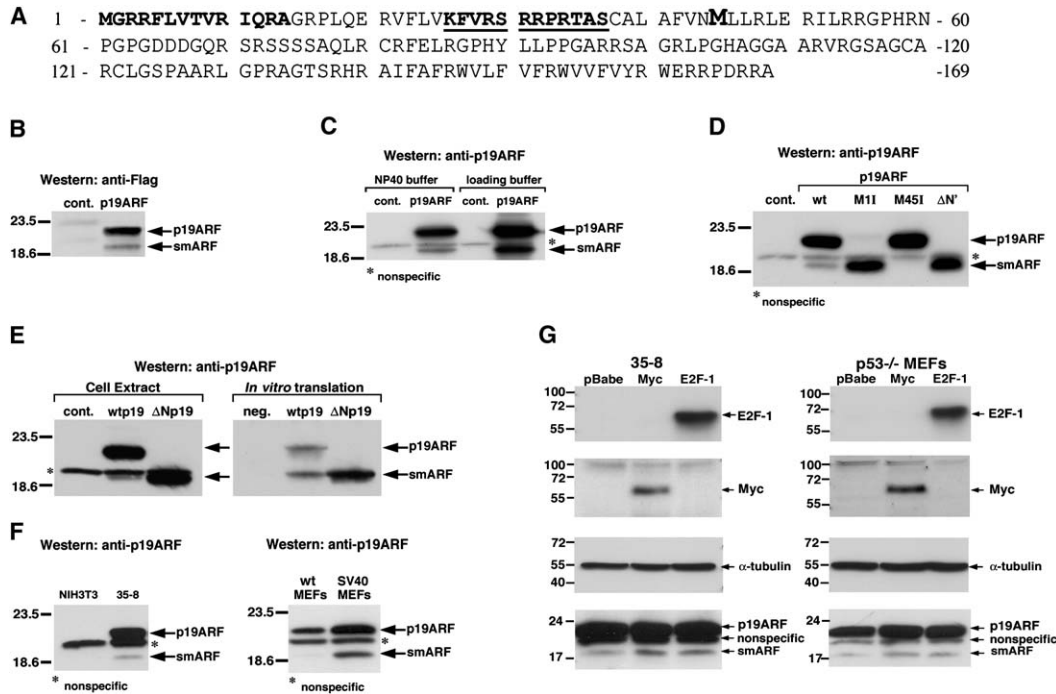


Figure 1. Internal Initiation of Translation Generates a Short Form of p19<sup>ARF</sup>

(A) Schematic representation of p19<sup>ARF</sup> protein sequence. Bold letters define the Mdm2 binding domains. The underlined segment (26–37) corresponds to the nucleolar localization signal. Met 45 is marked.

(B) Flag-tagged p19<sup>ARF</sup> was immunoprecipitated from 293T cells, 24 hr after transfection, with M2-Flag beads. Proteins were analyzed by Western blot of 12% gels using anti-Flag antibodies.

(C) 293T cells transfected with p19<sup>ARF</sup> for 24 hr were lysed with NP40 buffer or with sample loading buffer, and lysates were subjected to Western blot analysis on 12% gels with anti-p19<sup>ARF</sup> antibodies. The asterisk indicates the position of a nonspecific band crossreacting with the p19<sup>ARF</sup> antibody.

(D) Lysates from 293T cells transfected with wt p19<sup>ARF</sup>, p19<sup>ARF</sup> M11, p19<sup>ARF</sup> M45I, or ΔNp19<sup>ARF</sup> for 24 hr were analyzed by Western blot of 12% gels using anti-p19<sup>ARF</sup> antibodies.

(E) Wt p19<sup>ARF</sup> and ΔNp19<sup>ARF</sup> plasmids were subjected to an in vitro transcription/translation reaction, followed by immunoprecipitation with M2-Flag beads. The migration of the in vitro-translated polypeptides was compared to that of proteins extracted from transfected cells.

(F) Western blot analysis of extracts of the indicated cells (P2 wt MEFs or immortalized NIH3T3, 35-8, or SV40-transformed MEFs) reacted with anti-p19<sup>ARF</sup> antibodies. NIH3T3 cells, lacking the p19<sup>ARF</sup> locus, were used as a negative control.

(G) Early-passage (P5) p53 null MEFs or 35-8 cells were infected with retroviruses encoding c-Myc or E2F-1, or with an empty vector. Three days after selection, the expression levels of p19<sup>ARF</sup> forms were compared by Western blotting with p19<sup>ARF</sup>, Myc, E2F-1, and tubulin antibodies on 12% SDS-PAGE. This result was reproduced in three independent experiments.

identical to that of smARF, with almost no full-length p19<sup>ARF</sup> evident (Figure 1D). In contrast, conversion of Met45 to Ile (p19<sup>ARF</sup> M45I) abolished almost completely the presence of smARF, even though full-length p19<sup>ARF</sup> was produced efficiently (Figure 1D). As expected, substitution of both Met1 and Met45 by Ile abolished the expression of both isoforms (data not shown). Deletion of the first 40 amino acids of p19<sup>ARF</sup> generated a protein product with the same gel migration profile as the product of M11 (ΔNp19<sup>ARF</sup>, Figure 1D). In vitro translation in reticulocyte lysates further confirmed the existence of internal translation initiation. In vitro translation from the full-length p19<sup>ARF</sup> mRNA gave rise to two protein products. The shorter form had the same electrophoretic mobility on gels as the translation product of the ΔNp19<sup>ARF</sup> plasmid (Figure 1E, right panel) and as protein product expressed from this plasmid in transfected cells (compare left to right panel in Figure 1E). Interestingly, in the in vitro reaction, both proteins were produced in equal proportions, suggesting that translation from the second Met is as efficient as from the first. However,

in vivo, the short form comprises only a small fraction of the total. Thus, there must be additional regulatory mechanisms that influence translation rates or protein stability in vivo. A plasmid in which Met45 was converted to Ala (M45A) failed to produce smARF upon in vitro translation (data not shown). Taken together, the data suggest that the p19<sup>ARF</sup> open reading frame contains two initiation sites and that the primary mechanism for smARF production is internal initiation of translation at Met45.

This short form was also endogenously expressed in nontransfected cells. As shown in Figure 1F, the anti-p19<sup>ARF</sup> antibodies recognized a short p19<sup>ARF</sup> form that was present at low levels (compared to the full-length protein) in cells under steady-state growth conditions. This band was apparent in primary and immortalized mouse embryonic fibroblasts (i.e., in early passage [P2] of wt MEF cultures and in 35-8 cells that are MEF-derived immortalized cells that lack p53) but not in NIH3T3 cells which lack the INK4A/ARF locus. As expected, the electrophoretic mobility of the endogenous

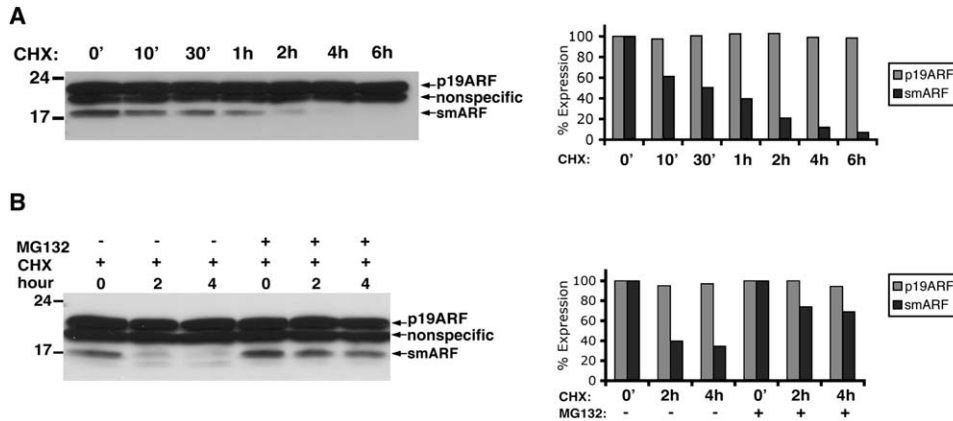


Figure 2. smARF Is Degraded Rapidly by the Proteasome

(A) 35-8 cells were treated with cycloheximide (20  $\mu$ g/ml) for the indicated times or remained untreated. The expression levels of p19<sup>ARF</sup> forms were compared by Western blotting using p19<sup>ARF</sup> antibody on 12% SDS-PAGE.

(B) Cells were treated with both cycloheximide and the proteasome inhibitor MG132 (100  $\mu$ M) for the indicated times. Cell lysates were analyzed as described for (A).

smARF was a bit faster than that of the recombinant Flag-tagged smARF (compare Figures 1C and 1F; the common nonspecific band can be used as an internal size reference).

Notably, smARF levels were elevated in response to ectopic expression of viral and cellular oncogenes. In SV40-transformed mouse embryonic fibroblasts, the expression of smARF increased more than 10-fold (Figure 1F, right panel). Additionally, introduction of two cellular oncoproteins, E2F-1 and c-Myc, into p53 null primary MEFs (P5) or into the 35-8 cell line led to an increase in smARF protein levels of 1.5- to 3-fold (Figure 1G). This moderate yet reproducible increase was also detected at the level of the p19<sup>ARF</sup> full-length protein, consistent with previous reports (Bates et al., 1998; Zindy et al., 1998). Thus, the two isoforms of p19<sup>ARF</sup> are subjected to upregulation in response to hyperproliferative signals of cellular and viral oncogenes.

#### smARF Is a Short-Lived Protein that Is Degraded by the Proteasome

We next examined whether the relative low steady-state levels of smARF are due to differences in the protein turnover. To this end, the stability of the two p19<sup>ARF</sup> forms following administration of cycloheximide was measured in the 35-8 cells. Notably, after as little as 10 min, smARF protein expression levels were already reduced, while the full-length p19<sup>ARF</sup> protein expression levels remained almost unchanged even after several hours of cycloheximide treatment (Figure 2A). Thus, smARF is a short-lived protein with a half-life of less than 1 hr, in contrast to the much more stable full-length p19<sup>ARF</sup>, which has been reported to display a half-life of ~6 hr (Kuo et al., 2004). Furthermore, the proteasome inhibitor MG132 significantly inhibited the turnover of smARF (Figure 2B), indicating that smARF's low steady-state levels are maintained by proteasome-mediated degradation. The significant difference in the turnover rates of the two translational products of ARF may explain why the ratio of smARF to full-length p19<sup>ARF</sup> is much lower in cells than in in vitro translation systems.

Of note, in the SV40-transformed fibroblasts shown in Figure 1F, the half-life of smARF was 2-fold greater than in the p53 null fibroblasts (data not shown).

#### The Human p14<sup>ARF</sup> mRNA Also Produces a Shorter Unstable Protein that Is Translated from an Internal ATG

The human ARF mRNA also contains an internal Met at position 48 (Figure 3A). In fact, in vitro translation of wt p14<sup>ARF</sup> in reticulocyte lysate gave rise to two protein products, the first corresponding to the full-length protein and the second to a faster migrating protein designated hsmARF (human smARF) that might correspond to translation initiation from Met 48 (Figure 3B). In vitro translation of a plasmid in which Met 1 was converted to Ala resulted in production of a protein product whose electrophoretic mobility was identical to that of hsmARF, with almost no full-length p14<sup>ARF</sup> evident (Figure 3B). In contrast, conversion of Met 48 to Ala significantly reduced the expression of hsmARF (data not shown). However, hsmARF was barely detectable in 293T cells upon transfection with the wt p14<sup>ARF</sup> plasmid, unless the proteasome inhibitor MG132 was added. Remarkably, after 17 hr of treatment with MG132, steady-state levels of hsmARF approached those of the full-length p14<sup>ARF</sup> (Figures 3C and 3D). These results indicate that the hsmARF's rapid turnover is mediated by the proteasome, even more efficiently than the murine smARF. hsmARF was detected by Western blotting with either anti-Flag (Figures 3C and 3D) or anti-p14<sup>ARF</sup> antibodies (data not shown), indicating that it contains an intact C terminus. As expected, expression of a p14 M1A plasmid in MG132-treated 293T cells resulted in abundant production of a protein product whose electrophoretic mobility was identical to that of hsmARF, with almost no full-length p14<sup>ARF</sup> evident. Thus, the production and controlled degradation of a short, internally initiated translation product are conserved properties of both the murine p19ARF and human p14<sup>ARF</sup> orthologs. This feature is not limited to human and mouse; the rat p19<sup>ARF</sup>, which we cloned and expressed in 293T cells,

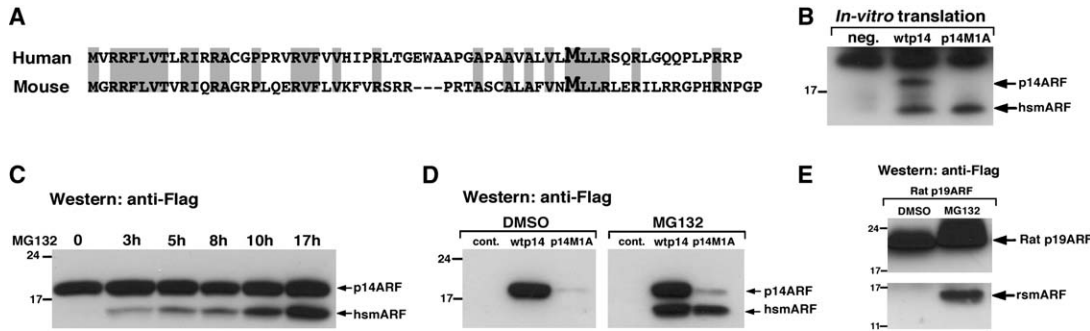


**Figure 3. The Human p14<sup>ARF</sup> mRNA Also Produces a Shorter Product that Is Rapidly Degraded**  
 (A) Schematic representation of the protein sequence of exon 1β of mouse p19<sup>ARF</sup> and human p14<sup>ARF</sup>. The human and mouse internal methionines are marked in bold, and a gap has been introduced to maximize regional alignment.  
 (B) Wt p14<sup>ARF</sup> and mutant p14<sup>ARF</sup> M1A plasmids were subjected to an in vitro transcription/translation reaction, followed by immunoprecipitation with M2-Flag beads. The proteins were separated by 15% SDS-PAGE. Western blot analysis was carried out using anti-Flag antibodies.  
 (C) 293T cells ectopically expressing p14<sup>ARF</sup> were treated with 10 μM MG132 for the indicated times, and lysates were subjected to Western blot analysis on 15% gels with anti-Flag antibodies.  
 (D) 293T cells ectopically expressing wt p14<sup>ARF</sup> or mutant p14<sup>ARF</sup> M1A plasmids were treated with DMSO or 10 μM MG132 for 17 hr. Cell lysates were analyzed as described for (C).  
 (E) 293T cells ectopically expressing rat p19<sup>ARF</sup> were treated with 10 μM MG132 for 17 hr. Proteins were separated by 15% SDS-PAGE and blotted to a nitrocellulose membrane, followed by probing with anti-Flag antibodies. Shown are two different exposures of the same blot in order to clearly visualize both full-length rat p19<sup>ARF</sup> and rsmARF.

also produced a short form that was readily detectable only upon proteasome inhibition (Figure 3E).

### smARF Localizes to Mitochondria

Two segments of p19<sup>ARF</sup>, namely residues 1–14 and 26–37, have been shown to be critical for the established functions of p19<sup>ARF</sup>, i.e., nucleolar localization, Mdm2 binding, and p53-dependent cell cycle arrest (Weber et al., 2000b) (see also Figure 1A). Additionally, the first 14 amino acids were recently shown to be essential for ARF-mediated inhibition of ribosomal RNA processing (Sugimoto et al., 2003), most probably through interaction with nucleophosmin/B23 (Bertwistle et al., 2004; Itahana et al., 2003). Since smARF lacks all these important functional domains, it may localize to other cellular compartments and function differently. To determine the localization of smARF, HeLa cells were transiently transfected with p19<sup>ARF</sup> M11, which mainly expresses smARF, and were immunostained with anti-Flag antibodies. Surprisingly, all transfected cells exhibited strong punctate cytoplasmic staining, and in most of the transfectants (>75%), no nucleolar staining was evident (Figure 4A, upper panels). To determine the nature of the punctate staining, the p19<sup>ARF</sup> M11 plasmid was co-transfected with the Mito-DsRed plasmid, which targets a red fluorescent protein specifically to the mitochondria due to its fusion with a mitochondrial targeting sequence. A perfect overlap between the anti-Flag staining and the Mito-DsRed signal was observed (Figure 4A), indicating that smARF localizes to mitochondria. smARF mitochondrial localization was also confirmed by confocal microscopy (data not shown). Notably, while HeLa cells cotransfected with luciferase, GFP, and Mito-DsRed plasmids exhibited the typical spread and tubular morphology of mitochondria (Figure 4A, lower panels), the morphology of the mitochondria in cells expressing smARF was abnormal; they were condensed, rounded, and clustered in the perinuclear region (Figure 4A). To confirm that the endogenous smARF

detected at low levels in 35-8 MEFs (see Figure 1F) also localizes to the mitochondria, these cells were costained with anti-p19<sup>ARF</sup> and anti-cytochrome c antibodies. Significantly, positive mitochondrial staining could be detected in a small fraction of the cells, in addition to the expected, much more prominent nucleolar staining of the full-length protein (Figure 4B). The staining was specific since no mitochondrial staining could be detected with the same antibodies in NIH3T3 cells that do not express any p19<sup>ARF</sup> (Figure 4B).

In order to confirm the mitochondrial localization of smARF by another approach, mitochondria were separated from the nuclear and cytosolic fractions by differential centrifugation. The biochemical cell fractionations were performed in 35-8 cells to assess endogenous proteins and in 293T cells transfected with ΔNp19<sup>ARF</sup> to assess ectopically expressed smARF; p19<sup>ARF</sup> M45A was used as a control. Proteinase K, a nonspecific serine protease that cannot penetrate mitochondrial membranes, was used to determine whether smARF is present inside the mitochondria or associates with the outer surface of the organelle. Both endogenous and exogenous smARF were detected predominantly in the Proteinase K-resistant compartment of the mitochondria (Figures 4C and 4D). smARF was subjected to degradation upon addition of the detergent Triton-X (Figure 4D). This pattern of resistance to Proteinase K was similar to that of cytochrome c (Figure 4D, left bottom lane), suggesting that smARF is an intramitochondrial protein. In contrast, Bcl-XL and Bcl-2, which are surface mitochondrial proteins, were completely exposed to Proteinase K even in the absence of detergent and therefore were completely proteolyzed (Figure 4D, right lanes). Of note, a minor portion of full-length p19<sup>ARF</sup> was present in the mitochondrial preparations (Figure 4C) and, in contrast to smARF, was sensitive to Proteinase K digestion (~80% digestion, Figure 4D). Therefore, it is possible that the presence of full-length p19<sup>ARF</sup> reflects non-specific contamination of the mitochondrial fraction,

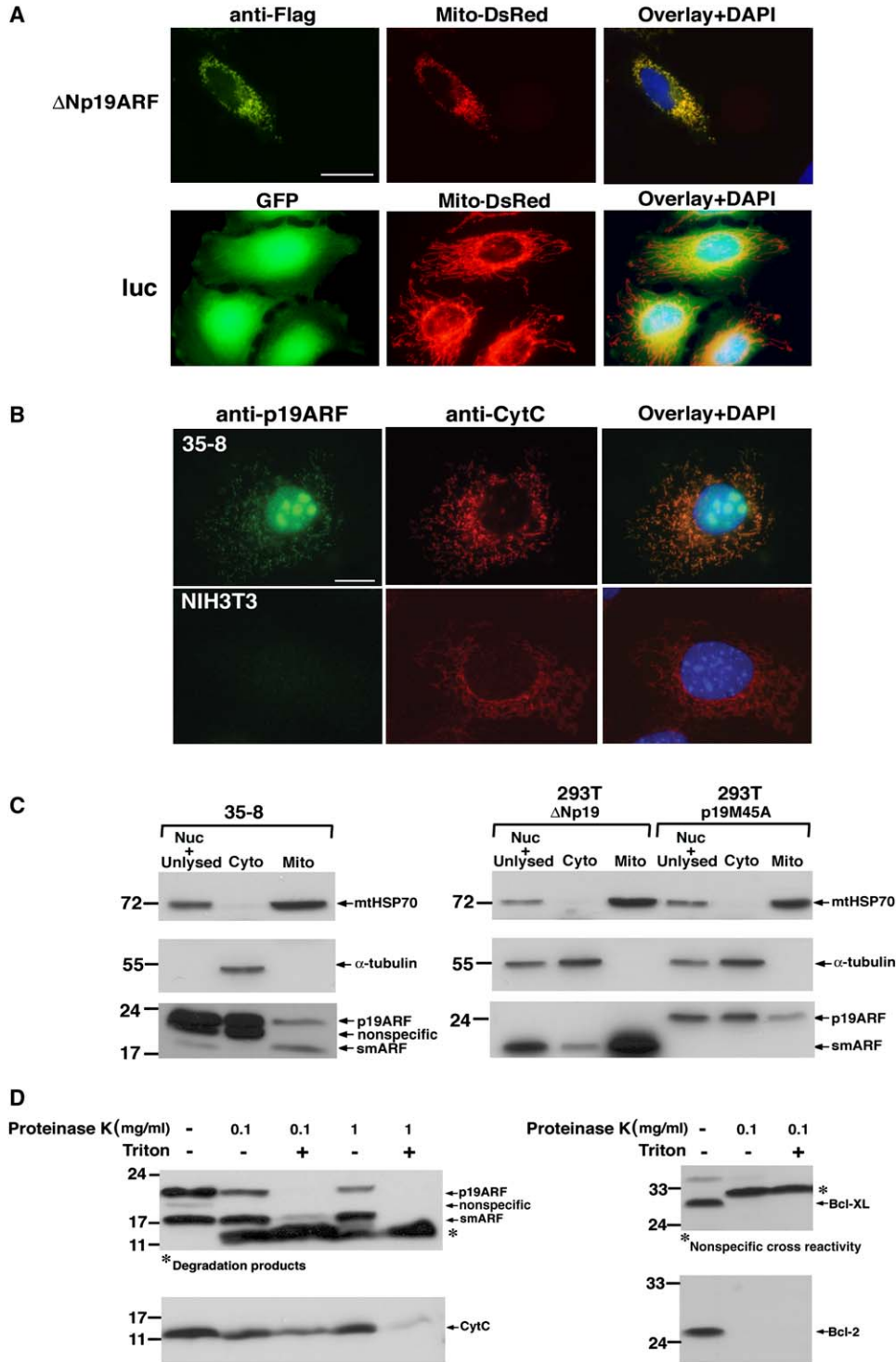


Figure 4. smARF Localizes to Mitochondria

(A) HeLa cells grown on glass coverslips were transiently cotransfected with Mito-DsRed and either p19<sup>ARF</sup> M11 or luciferase and GFP. After 24 hr, cells were immunostained with anti-Flag antibodies and examined by fluorescent light microscopy. Scale bar represents 10  $\mu$ m.

(B) A fraction of endogenous p19<sup>ARF</sup> also exhibits mitochondrial staining. 35-8 and NIH3T3 cells were immunostained with anti-p19<sup>ARF</sup> and anti-cytochrome c antibodies. Scale bar represents 5  $\mu$ m.

(C) smARF localizes within the mitochondria. Cellular extracts from 35-8 and 293T cells transfected with  $\Delta$ Np19<sup>ARF</sup> or p19<sup>ARF</sup> M45A were fractionated into nuclear, cytosolic, and mitochondrial fractions (40  $\mu$ g of each fraction of 35-8 cells per lane and 25  $\mu$ g of each fraction of 293T transfectants per lane). Note that the nuclear fraction was contaminated with unlysed cells. The enriched mitochondrial fraction was subjected to Proteinase K treatment (1 mg/ml). To assess the purity of the fractions, mtHSP70 and  $\alpha$ -tubulin were used as markers for the mitochondria and cytoplasm, respectively.

(D) The enriched mitochondrial fraction from 35-8 cells (100  $\mu$ g per lane) was assayed before and after Proteinase K treatment, in the presence or absence of Triton X-100 as indicated, and Western blotted for p19<sup>ARF</sup>, cytochrome c, Bcl-XL, and Bcl-2.

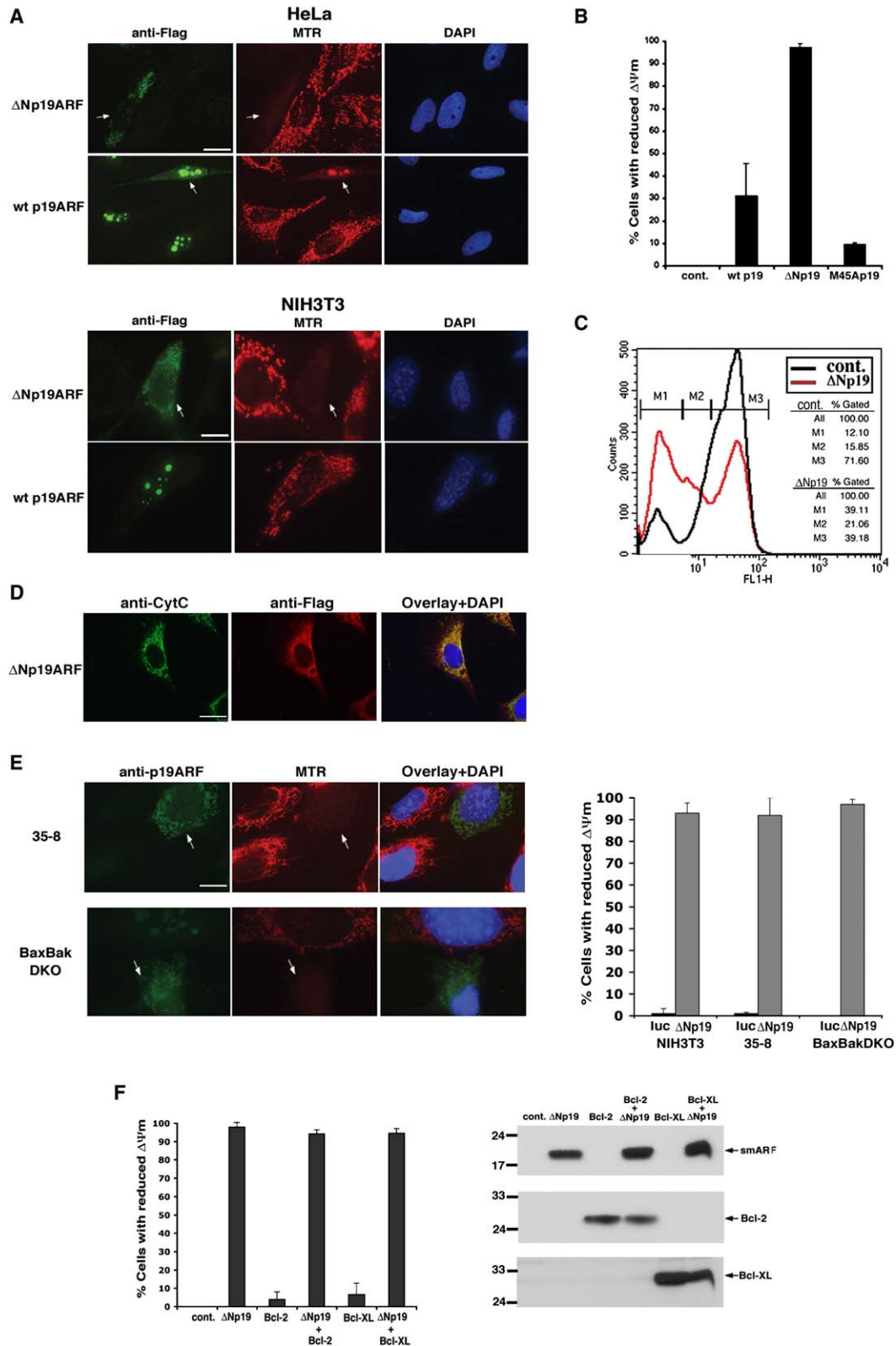


Figure 5. smARF Causes Dissipation of  $\Delta\Psi_m$  in a p53- and Bcl-2-Family-Independent Manner

(A) HeLa or NIH3T3 cells were transiently transfected for 24 hr with the indicated plasmids, incubated for 30 min with MitoTracker Red, immunostained with anti-Flag antibodies, and viewed by fluorescent light microscopy. The arrows indicate transfected cells that fail to exhibit MitoTracker Red staining. Scale bar represents 5  $\mu$ m.

(B) Quantitation of NIH3T3 cells exhibiting reduced  $\Delta\Psi_m$ , as analyzed in (A). Data presented are the mean  $\pm$ SD calculated from triplicates of 100 transfected cells each.

while smARF's resistance to Proteinase K indicates that it is a genuine resident of the mitochondria.

### smARF Causes Dissipation of $\Delta\Psi m$

To assess possible effects of smARF on mitochondrial function, a fluorescent mitochondrial dye, MitoTracker Red (CMX-Ros, Molecular Probes), which accumulates only in actively respiring mitochondria that have an intact  $\Delta\Psi m$ , was used. HeLa and NIH3T3 cells expressing either wt p19<sup>ARF</sup> or  $\Delta Np19^{ARF}$  were stained with MitoTracker Red, fixed, and then immunostained with anti-Flag antibodies. Surprisingly, nearly 100% of cells transfected with the  $\Delta Np19^{ARF}$  plasmid lacked MitoTracker dye uptake, while nontransfected neighboring cells exhibited strong MitoTracker staining (Figure 5A). Unlike the  $\Delta Np19^{ARF}$ -expressing cells, the adjacent nontransfected cells displayed the typical spread and tubular morphology of mitochondria. These observations suggested that smARF not only impairs the structure of the mitochondria but also dramatically dissipates  $\Delta\Psi m$ . These data were compared to the outcome of transfections with the wt p19<sup>ARF</sup> plasmid, which expresses high levels of full-length p19<sup>ARF</sup> and small amounts of smARF. As expected, most of the cells displayed the typical p19<sup>ARF</sup> nucleolar staining and strong MitoTracker staining, suggesting that  $\Delta\Psi m$  in these transfectants was not impaired (Figure 5A). Yet, in a small fraction of the transfected cells, mainly those displaying the highest p19<sup>ARF</sup> expression levels, extranuclear staining was evident in addition to the nucleolar distribution; in some of those cells, MitoTracker uptake was reduced (Figure 5A). This further supports the conclusion that the mitochondrial presence of smARF causes dissipation of  $\Delta\Psi m$ . Figure 5B shows a quantitative comparison of the extent of loss of  $\Delta\Psi m$  in NIH3T3 cells expressing full-length p19<sup>ARF</sup>,  $\Delta Np19^{ARF}$ , or p19<sup>ARF</sup> M45A. The proportion of cells exhibiting reduced  $\Delta\Psi m$  correlated with the levels of smARF produced:  $\Delta Np19^{ARF}$ , which produces large amounts of the short form only, caused loss of MitoTracker staining in nearly 100% of transfected cells, while  $\Delta\Psi m$  was intact in most of the cells transfected with p19<sup>ARF</sup> M45A, which expresses almost exclusively full-length p19<sup>ARF</sup>. An intermediate phenotype (30%) was observed with the wt p19<sup>ARF</sup> plasmid, which is capable of producing both forms. Thus, these experiments imply that smARF, but not full-length p19<sup>ARF</sup>, is capable of mediating the reduction in  $\Delta\Psi m$  and that the ectopically expressed smARF has to exceed some threshold levels in order

to damage the mitochondria. To confirm that the loss of MitoTracker Red staining was in fact a result of smARF-mediated reduction in  $\Delta\Psi m$ , flow cytometric analysis of transfected NIH3T3 cells stained with the mitochondrial probe DiOC<sub>6</sub> was performed. FACS analysis was performed on the entire cell population (~50% transfection efficiency). smARF caused a complete loss of  $\Delta\Psi m$  in 39.1% of the total cells (i.e., in most of the transfectants) (Figure 5C). Thus, two independent experimental methods prove that smARF induces dissipation of the  $\Delta\Psi m$ . Despite loss of  $\Delta\Psi m$  at 24 hr, cytochrome c was not released from the mitochondria in the majority of cells (Figure 5D), indicating that the outer mitochondrial membrane was intact. Notably, hsmARF was also detected in the mitochondria and caused dissipation of the  $\Delta\Psi m$  (data not shown).

### smARF Damages $\Delta\Psi m$ in a p53- and Bcl-2-Independent Manner

In order to test whether smARF's function is coupled to the known mitochondrial signaling pathways that involve p53 and the Bcl-2 family proteins, the mitochondrial effect of smARF was assessed in the presence and absence of these regulators. It was found that smARF was also capable of reducing the  $\Delta\Psi m$  in the 35-8 MEF-derived cell line that is p53 deficient (Figure 5E), indicating that p53 is not required for the mitochondrial effects of this p19<sup>ARF</sup> form. Introduction of  $\Delta Np19^{ARF}$  into Bax/Bak double null MEFs likewise resulted in dissipation of  $\Delta\Psi m$  (Figure 5E). Furthermore, smARF's ability to dissipate  $\Delta\Psi m$  was not impaired by overexpressing either Bcl-2 or Bcl-XL (Figure 5F). This indicates that smARF damages the mitochondrial membrane in a manner that involves neither p53 nor the Bcl-2 family.

### smARF Induces Autophagy and Caspase-Independent Cell Death

In order to assess the cellular outcome of smARF expression, 293T cells were transfected with  $\Delta Np19^{ARF}$  and were further analyzed at 48 hr. Cells transfected with control plasmid reached near confluency (Figure 6A). In contrast, culture dishes transfected with  $\Delta Np19^{ARF}$  contained many rounded, floating, dying cells, similar to cultures that were transfected with TNFR-1 (p55 tumor necrosis factor receptor-1), which triggers typical caspase-dependent cell death (Figure 6A). The drop in cell survival in response to  $\Delta Np19^{ARF}$  transfection was further quantified at 72 hr

(C) NIH3T3 cells expressing luciferase (black) or smARF (red) were assayed for loss of  $\Delta\Psi m$  24 hr after transfection by flow cytometric analysis of DiOC<sub>6</sub> fluorescence. Histograms represent cell counts versus fluorescence intensity. Three distinct populations of cells were defined by their levels of fluorescent intensities: M1 cells with dramatic reduction in  $\Delta\Psi m$ , M2 cells with an intermediate state of  $\Delta\Psi m$ , and M3 cells with intact  $\Delta\Psi m$ . Note that the transfection efficiency, as determined by the percent of GFP-positive cells, was 50%, but the entire cell population, comprising both transfected and nontransfected cells, was analyzed.

(D) NIH3T3 cells were transiently transfected for 24 hr with  $\Delta Np19^{ARF}$  plasmid, immunostained with anti-cytochrome c and rabbit anti-Flag antibodies, and viewed by fluorescent light microscopy. Scale bar represents 5  $\mu m$ .

(E) 35-8 cells and Bax/Bak double knockout immortalized MEFs were transiently transfected for 24 hr with the  $\Delta Np19^{ARF}$  plasmid, stained with MitoTracker Red and anti-p19<sup>ARF</sup> antibodies, and viewed by fluorescent light microscopy. The arrows indicate transfected cells that failed to exhibit MitoTracker Red staining. Scale bar represents 5  $\mu m$ . The graph represents quantitation of transfected cells exhibiting loss of mitochondrial potential upon transfection of NIH3T3, 35-8 cells, and Bax/Bak double knockout immortalized MEFs with either luciferase or  $\Delta Np19$  together with GFP. Data presented are the mean  $\pm$ SD calculated from triplicates of 100 transfected cells each.

(F) NIH3T3 cells were cotransfected with luciferase or  $\Delta Np19^{ARF}$  and either Bcl-2 or Bcl-XL together with GFP. After 24 hr, cells were stained with MitoTracker Red. GFP-positive cells were visualized by fluorescent microscopy and scored for the reduction in MitoTracker staining. Data presented are the mean  $\pm$ SD calculated from triplicates of 100 transfected cells each. Western blot analysis verified the ectopic expression of the transfected plasmids.

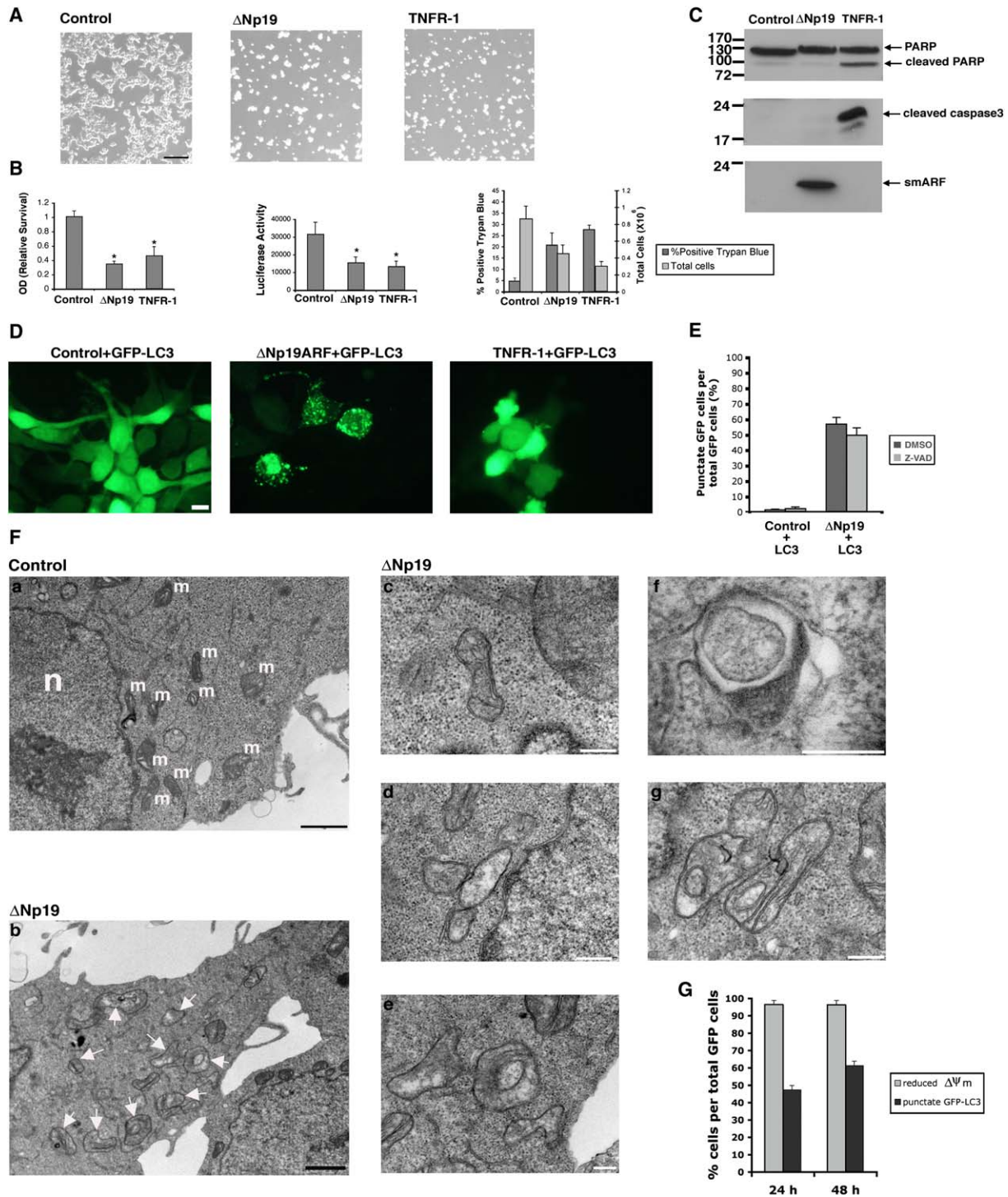


Figure 6. smARF Induces Cell Death that Involves Autophagic Vesicle Formation

(A) Representative photographs of cells 48 hr after transfection with CAT,  $\Delta$ Np19<sup>ARF</sup>, or TNFR-1 plasmids. Transfection efficiency corresponded to ~90%. Scale bar represents 200  $\mu$ m.

(B) Quantification of cell viability 72 hr after transfection with control,  $\Delta$ Np19<sup>ARF</sup>, or TNFR-1, using Neutral Red assay in 293T cells (left panel) or luciferase activity assay in 293-Luc cells (middle panel). The right panel represents quantitation of cell death as measured by assessing the percent of trypan blue-positive cells out of total cells. Total cell number is also shown. Data presented are the mean  $\pm$ SD of triplicate plates and are representative of three independent experiments. The asterisk denotes significance level of  $p < 0.02$ .

(C) Western blot analysis of extracts of the indicated transfected 293T cells, reacted with anti-PARP, anti-cleaved caspase-3, or anti-Flag antibodies.

(D) Localization of GFP-LC3 in cells cotransfected with either luciferase,  $\Delta$ Np19<sup>ARF</sup>, or TNFR-1. Scale bar represents 40  $\mu$ m.

(E) Quantitation of the percentage of cells with punctate GFP-LC3 fluorescence per total GFP-LC3-positive cells, 48 hr after transfection, in the presence or absence of zVAD-fmk. Data presented are the mean  $\pm$ SD of triplicate plates.

and compared to the outcome of transfection with TNFR-1. Two independent viability assays were used, the Neutral Red dye uptake assay and a second sensitive assay that measures cellular luciferase activity in viable cells. As shown in Figure 6B, smARF reduced cell viability to a similar extent as TNFR-1. In parallel, the extent of cell death was directly measured by trypan blue staining. A significant increase in the percent of trypan blue-positive cells was observed in  $\Delta$ Np19<sup>ARF</sup> transfectants, similar to the extent of cell death induced by TNFR-1 (Figure 6B, right panel). Yet, molecular analysis revealed that the type of cell death is different in each case. Western blot analysis of PARP-1 and caspase-3 cleavage confirmed that TNFR-1 induced classical apoptotic cell death involving caspase activation (Figure 6C). smARF, in contrast, induced caspase-independent cell death, which was not accompanied by PARP-1 or caspase-3 cleavage (Figure 6C) and which was not blocked by the pancaspase inhibitor zVAD-fmk (data not shown). Although mitochondrial function was impaired by smARF (Figure 5), ATP production was maintained in these cells (data not shown), probably by glycolysis, suggesting that cell death is not a result of ATP depletion.

Further characterization of the cell death phenotype suggested that smARF activates autophagy. This was first assessed by examining the localization of GFP-tagged LC3 (microtubule-associated protein 1 light chain 3). Vesicular accumulation of LC3 is a marker of autophagy, as recruitment of modified LC3 to the nascent autophagic vesicle is an early event in autophagosome formation (Kabeya et al., 2000). To this end, the GFP-tagged LC3 plasmid was coexpressed with either an irrelevant control plasmid or with  $\Delta$ Np19<sup>ARF</sup> or TNFR-1 plasmids. Diffuse cytoplasmic localization of GFP-LC3 was observed when it was expressed together with the control or with the TNFR-1 plasmids, whereas around 60% of the cells that expressed smARF showed punctate fluorescent staining indicative of autophagic vesicles (Figure 6D). Furthermore, the number of autophagic cells showing punctate staining of LC3 was not significantly reduced upon administration of the pancaspase inhibitor zVAD-fmk (Figure 6E). The presence of autophagic vesicles was further confirmed by examination of 293T transfectants by transmission EM (TEM). As expected, in control-transfected cells, autophagic vesicles were rarely observed (Figure 6Fa). In contrast, numerous double membrane-enclosed vesicles surrounding cytoplasmic matter and organelles appeared in  $\Delta$ Np19<sup>ARF</sup>-transfected cells (Figures 6Fb–6Fg).

To determine the relative kinetics with which the different smARF-induced events occurred, 293T cells were cotransfected with  $\Delta$ Np19<sup>ARF</sup> together with GFP-LC3 and were stained with MitoTracker Red at the indicated times. Most of the cells (96%) exhibited reduced  $\Delta\Psi m$  as early as 24 hr after transfection (Figure 6G). In contrast, autophagic vesicles accumulated more slowly. Punctate localization of GFP-LC3 was first observed at

24 hr in 47% of the cells and reached a value of 61% after 48 hr (Figure 6G). Thus, the disruption of  $\Delta\Psi m$  clearly precedes the development of autophagy in smARF-expressing cells.

### Knockdown of Endogenous Autophagic Proteins Protects against smARF-Induced Cell Death

Recent studies have documented several scenarios in which induction of autophagy triggers cell death (Mills et al., 2004; Shimizu et al., 2004; Yu et al., 2004) while in many other cellular settings autophagy is cytoprotective (reviewed by Gozuacik and Kimchi [2004]). To assess the involvement of autophagy in smARF-induced cell death, shRNA plasmids were generated to target two key mediators of autophagosome formation, ATG5 and Beclin-1. ATG5 is part of a ubiquitin-like pathway necessary for the formation of the autophagic vesicle. It is covalently conjugated to ATG12, enabling the formation of a large multiprotein complex that is recruited to the nascent autophagosomal membrane (Mizushima et al., 2001). Beclin-1 is a regulator of a class III phosphatidylinositol 3-kinase complex, which is involved in the nucleation of the autophagosomes (Liang et al., 1999). Both ATG5 and Beclin-1 protein levels were partially reduced upon transfection with the shRNA constructs (Figure 7A). The reduction in protein expression was functionally significant since, as expected, the ATG5 or Beclin-1 shRNAs partially reduced autophagosome formation by amino acid deprivation (Figure 7B). To assess the effect of ATG5 or Beclin-1 reductions on smARF-induced autophagy, 293T cells in which ATG5 or Beclin-1 was knocked down were cotransfected with GFP-LC3 and  $\Delta$ Np19<sup>ARF</sup>. It was found that the extent of autophagy induced by smARF was partially reduced by knocking down either ATG5 or Beclin-1 in a statistically significant manner (Figure 7C). To determine whether autophagy is causative to the smARF-induced cell death, or is rather a cytoprotective mechanism, we measured the outcome of knockdown of ATG5 or Beclin-1 on cell viability. To this end, 293-Luc cells in which ATG5 or Beclin-1 protein levels were reduced by the shRNA plasmids were subsequently transfected with control or  $\Delta$ Np19<sup>ARF</sup> plasmids, and the survival assay was performed 72 hr later. It was found that the knockdown of the autophagic proteins attenuated rather than increased the ability of smARF to induce cell death (Figure 7D). This result was obtained repeatedly in three independent experiments. Western blotting confirmed that equal levels of smARF were expressed in all transfectants (Figure 7A). Thus, the massive autophagy that is induced by smARF positively contributes to the cell death process.

### Discussion

This work highlights a new mode of regulation of p19<sup>ARF</sup> expression that occurs at the level of translation and confers a nonnucleolar death-inducing function to p19<sup>ARF</sup>. It involves the production of a previously

(F) Transmission electron micrographs of 293T cells transfected with luciferase (a) or  $\Delta$ Np19<sup>ARF</sup> ([Fb–Fg]; [Fe] is a magnification of [Fb]). The “m” indicates mitochondria, the “n” indicates nucleus. The black bar represents 1  $\mu$ m, the white bar represents 200 nm. White arrows point to autophagic vesicles.

(G) Quantitation of 293T cells cotransfected with GFP-LC3 and  $\Delta$ Np19<sup>ARF</sup> plasmids exhibiting reduced  $\Delta\Psi m$  and punctate GFP-LC3 fluorescence per total GFP-LC3-positive cells at the indicated times. Data presented are the mean  $\pm$ SD of triplicate plates.

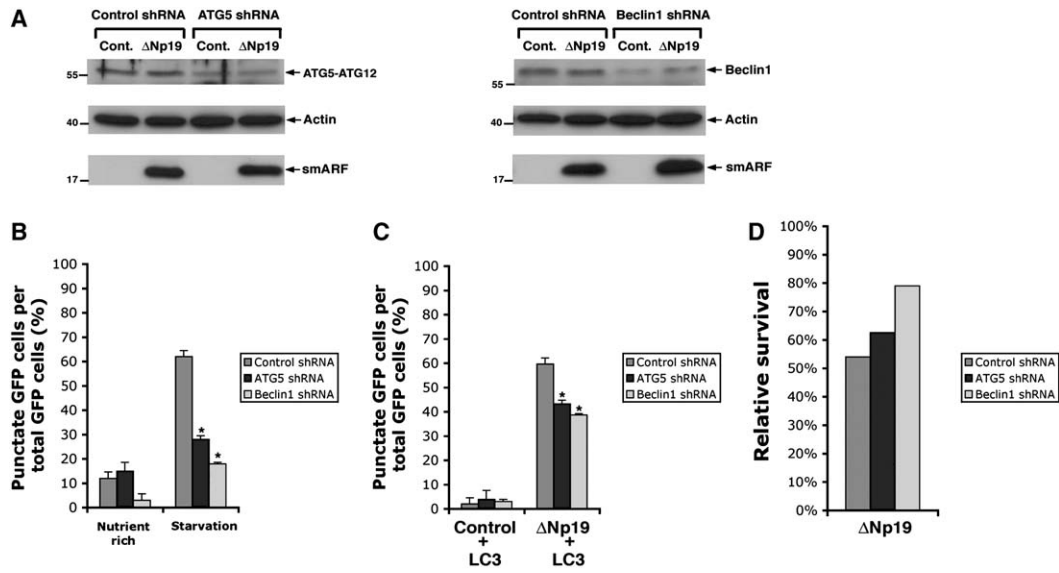


Figure 7. Knockdown of Endogenous Autophagic Proteins Protects against smARF-Induced Cell Death

(A) 293-Luc cells were transfected with control, ATG5, or Beclin-1 shRNA plasmids. After 48 hr, the cells were retransfected with control (CAT) or  $\Delta$ Np19<sup>ARF</sup> plasmids. Western blot analysis was performed 72 hr later, with anti-ATG5, anti-Beclin-1, or anti-Flag antibodies. Actin was used as a loading control.

(B) 293T cells were transfected with control, ATG5, or Beclin-1 shRNA plasmids. After 4 days, the cells were cotransfected with GFP-LC3. Twenty-four hours later, the cells were starved in EBSS for 3 hr at 37°C. The cells with punctate GFP-LC3 were quantified per total GFP-LC3-positive cells. Data presented represent mean  $\pm$ SD calculated from triplicates of 100 transfected cells each. The asterisk denotes significance level of  $p < 0.001$ .

(C) 293T cells were transfected with control, ATG5, or Beclin-1 shRNA plasmids. After 4 days, the cells were cotransfected with GFP-LC3 and control or  $\Delta$ Np19<sup>ARF</sup> plasmids. Twenty-four hours later, the cells with punctate GFP-LC3 were quantified per total GFP-LC3-positive cells. Data presented represent mean  $\pm$ SD calculated from triplicates of 100 transfected cells each. The asterisk denotes significance level of  $p < 0.001$ .

(D) 293 cells that stably express luciferase (293-Luc) were transfected with the indicated shRNA plasmids. After 48 hr, the cells were retransfected with control (CAT) or  $\Delta$ Np19<sup>ARF</sup> plasmids, and the survival assay was performed 72 hr later. The overall cell survival was determined by dividing the average luciferase activity values (from triplicates) of cells transfected with  $\Delta$ Np19<sup>ARF</sup> by the average values of the cells transfected with control for each knockdown.

uncharacterized translation product, smARF, which results from internal initiation at Met45. This form lacks the N-terminal region encompassing the domains required for the various nucleolar functions of p19<sup>ARF</sup> and, instead, translocates to a Proteinase K-resistant compartment of the mitochondria. In healthy cells, smARF accumulates to low steady-state levels, due to its rapid turnover, and thus is not harmful to cells. Forced expression of this form, however, leads to dissipation of the  $\Delta\Psi_m$  and ultimately to autophagic vesicle formation and caspase-independent cell death.

smARF causes the dissipation of the inner membrane potential by a mechanism that does not involve the different Bcl-2 family members that were examined. Furthermore, no signs of cytochrome c release into the cytoplasm and subsequent caspase activation were detected, suggesting that the outer membrane is not damaged by smARF. Thus smARF does not trigger type I caspase-dependent cell death. Instead, smARF induced the formation of autophagosomes. Autophagy can be used by cells to protect them from adverse conditions or alternatively may lead to their final destruction (reviewed by Gozuacik and Kimchi [2004]). The electron microscopy studies performed here showed that smARF induces a large number of autophagosomes in cells, which engulf different intracellular components including mitochondria, ER, and bulk cytoplasm. Knockdown two important elements in the autophagy

pathways, ATG5 and Beclin-1, partially compromised both autophagic activity and cell death, implying that autophagy is necessary for smARF-induced cell death. Several studies suggest that damaged mitochondria may be a trigger for the induction of autophagy (Elmore et al., 2001; Rodriguez-Enriquez et al., 2004). In particular, in yeast grown under nonstarvation conditions, autophagy can be induced by impairing the mitochondrial electrochemical transmembrane potential (Priault et al., 2005). Thus, it is possible, although not yet proven, that the smARF-induced mitochondrial depolarization may signal the induction of autophagic vesicle formation. Since ATP levels were not reduced in smARF-expressing cells, it is unlikely that the signaling operates through induction of AMP kinase (AMPK) and mTOR inhibition.

Ectopic expression of cellular and viral oncogenes led to elevation of smARF protein levels, suggesting that both the nucleolar full-length p19<sup>ARF</sup> and the mitochondrial short form are regulated by oncogenes. The existence of these two isoforms of p19<sup>ARF</sup> may thus enable hyperproliferative signals to activate two concurrent pathways that may both contribute to the cell's defensive response to transformation. The first pathway involves the known nucleolar functions of the full-length protein, i.e., regulation of p53 stability and activity by binding to Mdm2 (Honda and Yasuda, 1999; Midgley et al., 2000; Tao and Levine, 1999; Weber et al., 1999) and interference with the processing and maturation of

preribosomal RNA, thereby restraining protein synthesis and cell growth (Bertwistle et al., 2004; Itahana et al., 2003; Sugimoto et al., 2003). The second pathway, activated by the short form, utilizes a mitochondria-based mechanism to induce autophagy and caspase-independent cell death. This mitochondrial pathway may act as a back-up to the nuclear pathway, particularly in circumstances when p53 and/or the caspase-dependent apoptotic pathway are nonfunctional.

It is noteworthy that in response to DNA damage, a fraction of p53 may also localize to the mitochondria and activate a mitochondrial-based death pathway, yet by a different mechanism that involves Bcl-2 family members (Mihara et al., 2003). Furthermore, p53 was recently linked to autophagy by activating AMPK and inhibiting mTOR activity upon glucose deprivation and is also a target for activation by AMPK (Feng et al., 2005; Jones et al., 2005). However, those mechanisms do not appear to bear any relationship to the ARF activity described in the present study.

Notably, the human p14<sup>ARF</sup> ortholog is also capable of producing hsmARF, which can localize to and impair the mitochondria, despite its retention of a second nucleolar localization signal (Weber et al., 2000b). Thus the mitochondrial function of ARF is conserved between the disparate human and mouse orthologs. A comparison of sequence databases revealed, however, that while the human, mouse, and hamster genes all have a second Met at a similar position, there is no corresponding Met in the published sequences from other species such as rat, opossum, and pig. Yet, expression of the cDNA for rat p19<sup>ARF</sup> produced a shorter form of the protein in the presence of proteasome inhibition, similar to what was observed for the human protein. Thus, while it is likely that the rat ortholog utilizes another mechanism to generate its short form, the production of smARF is conserved among mammals, suggesting that this form serves an essential cellular function.

In summary, an already complex picture involving the existence of alternative reading frames of the INK4A/ARF locus has now become even more exciting with the discovery of an alternative translation product of the ARF mRNA. The interesting activities associated with this short ARF isoform may in fact be critical to ARF's tumor suppressor function.

## Experimental Procedures

### DNA Constructs, Transfections, and Infections

All cell lines were grown as previously described (Cohen et al., 1997; Raveh et al., 2001). 293T and HeLa cells were transiently transfected by the standard calcium phosphate technique. NIH3T3 cells, 35-8 cells, and Bax/Bak double knockout immortalized MEFs were transiently transfected with Lipofectamine (Invitrogen). Retroviral mediated infections were performed as previously described (Cohen et al., 1997; Raveh et al., 2001). To induce autophagy by amino acid deprivation, cells were washed twice with PBS and then incubated in Earle's balanced salt solution (EBSS, Biological Industries) for 3 hr at 37°C. p19<sup>ARF</sup> and p14<sup>ARF</sup> were expressed from pcDNA3 plasmids tagged at their C terminus with the Flag epitope. Methionine substitution mutants were generated by site-directed mutagenesis (QuikChange Site-Directed Mutagenesis Kit, Stratagene). Rat p19<sup>ARF</sup> was cloned from a rat bladder cDNA library (kind gift of N. Dekel, Weizmann Institute of Science) by PCR using primers corresponding to accession number AY679727, with a Flag tag at the 3' end of the cDNA. To generate pSUPER-based shRNA vectors tar-

geting Beclin-1, ATG5, and HcRed (control), 19-mer oligos corresponding to nucleotides 1339–1357 of Beclin-1 (accession number NM003766), 779–797 of ATG5 (accession number NM004849) (Boya et al., 2005), and 99–117 of HcRed (accession number AF363776) were annealed and ligated into the BglIII and HindIII of the pSUPER vector (Brummelkamp et al., 2002). Myc and E2F-1 were produced from pBabe-puro-derived retroviruses that were used to infect cells under puromycin selection conditions as previously described (Raveh et al., 2001). Cells were viewed live on an inverted IX70 microscope (Olympus) equipped with a CPlan 10× objective (N.A. 0.25) and a DVC digital camera (Digital Video Camera Co.). Images were captured using the C-View V2.1 imaging program and processed with Adobe Photoshop.

### Protein Analysis

Cell lysis, immunoprecipitations, and immunoblotting were done as previously described (Raveh et al., 2001). Proteins were separated on 10%, 12%, or 15% SDS-PAGE. The following monoclonal antibodies were used: anti Flag, anti  $\alpha$ -tubulin, and anti actin (Sigma); anti c-Myc, anti E2F-1, and anti Bcl-2 (Santa Cruz Biotechnology); anti cytochrome c (BD Biosciences); and anti PARP (BIOMOL). Polyclonal antibodies to p19<sup>ARF</sup> (Abcam); mitochondrial HSP70/GRP75, Bcl-XL, and Beclin-1 (Santa Cruz Biotechnology); cleaved caspase-3 (Cell Signaling); and ATG5 (a generous gift from N. Mizushima) were used. Detection was done by either HRP-conjugated goat anti-mouse or anti-rabbit secondary antibodies (Jackson ImmunoResearch), followed by enhanced chemiluminescence (SuperSignal, Pierce)

### In Vitro Transcription and Translation Assay

Wt p19<sup>ARF</sup>, p19<sup>ARF</sup> mutant, wt p14<sup>ARF</sup>, and p14<sup>ARF</sup> mutant plasmids were used as templates for coupled in vitro transcription/translation from the T7 promoter (TNT Reticulocyte Lysate Systems, Promega) by conventional procedures, using a complete amino acid mixture. The reaction products were immunoprecipitated with M2-Flag beads and then subjected to Western blot analysis on 12% or, where indicated, 15% gels.

### Analysis of Protein Stability In Vivo

The turnover of the endogenous smARF in 35-8 cells was monitored by Western blot analysis of cell extracts following the addition of 20  $\mu$ g/ml cycloheximide (Sigma). In addition, when indicated, the proteasome inhibitor MG132 (Calbiochem; 10  $\mu$ M or 100  $\mu$ M) was included.

### Cell Fractionation and Proteinase K Sensitivity Assays

Cell pellets were suspended in isotonic HIM buffer (200 mM mannitol, 70 mM sucrose, 1 mM EGTA, 10 mM HEPES [pH 7.5]) with protease inhibitors, incubated 10 min on ice, homogenized by multiple passages through a 25G needle, and centrifuged at 300  $\times$  g at 4°C for 10 min to pellet the nuclear fraction. To reduce the amount of unlysed cells in the nuclear fraction, the homogenization procedure was repeated twice in the nuclear fraction. The final pellets were extracted with PLB buffer containing protease inhibitors (nuclear fraction). The supernatant (S1) was recentrifuged at 10,000  $\times$  g at 4°C for 10 min to pellet mitochondria, and the supernatant was saved as the cytosolic fraction. Unless indicated otherwise, the crude mitochondria fraction was resuspended in HIM buffer and treated for 30 min with Proteinase K (0.1 or 1 mg/ml) in the presence or absence of Triton X-100 (1% final concentration). Proteolysis was stopped by the addition of 5 nM PMSF. The mitochondrial pellets were extracted with PLB buffer containing protease inhibitors to give the mitochondrial fraction.

### Immunostaining

Wt p19<sup>ARF</sup> and derived mutants were transfected into HeLa, NIH3T3, 35-8, 293T cells, or Bax/Bak double knockout MEFs grown on glass coverslips. When indicated, after 24 hr the cells were treated with 100 nM MitoTracker dye (CMX-Ros, Molecular Probes) in growth medium for 30 min at 37°C and then fixed and permeabilized by subsequent incubations in 3.7% formaldehyde, methanol, and acetone. Cells were then permeabilized/blocked with 0.4% Triton-X 100 (Sigma) in 10% normal goat serum (Biological Industries) and incubated for 1 hr with mouse anti-Flag antibodies (Sigma), followed by FITC-conjugated donkey anti-mouse secondary antibodies

(Jackson ImmunoResearch) or rabbit polyclonal anti-Flag (Sigma), followed by rhodamine-RedX (RRX)-conjugated goat anti-rabbit (Jackson ImmunoResearch). To stain endogenous p19<sup>ARF</sup>, 35-8 cells and NIH3T3 cells were permeabilized with 0.5% Triton-X-100 in 4% paraformaldehyde solution for 5 min and then fixed with paraformaldehyde for 20 min. Cells were incubated with antibodies to p19<sup>ARF</sup> (Abcam) or cytochrome c (BD Biosciences) and then incubated with Cy-2-conjugated donkey anti-rabbit antibodies or Rhodamine-conjugated goat anti-mouse antibodies (Jackson ImmunoResearch). Cells were finally stained with DAPI (0.5 µg/ml, Sigma). To visualize autophagosomes, 293T cells grown on glass coverslips in the presence or absence of 100 µM zVAD-fmk (Sigma) were cotransfected with 1 µg GFP-LC3 and 9 µg luciferase,  $\Delta$ Np19<sup>ARF</sup>, or TNFR-1 expression plasmids. Stained cells were viewed by fluorescent microscopy (Olympus BX41) with 60× (N.A. 1.25) or 100× (N.A. 1.3) UPlan-FI oil immersion objectives, and digital images were obtained with a DP50 CCD camera using Viewfinder-Lite and StudioLite software (Olympus). Composites and merged images were generated in Photoshop (Adobe Systems).

#### Flow Cytometric Analysis of $\Delta\Psi m$

Perturbations in  $\Delta\Psi m$  were monitored by flow cytometry. Transfected NIH3T3 cells were collected in culture medium by trypsinization and stained with 40 nM 3,3'-dihexyloxycarbocyanine (DiOC<sub>6</sub>, Sigma) for 30 min at 37°C. Samples were then analyzed by a FACScan cytometer (Becton Dickinson), using an excitation laser of 488 nm and emission filter of 530/30 nm.

#### Viability Assays

For the Neutral Red assay, 293T cells were transfected with control (CAT),  $\Delta$ Np19<sup>ARF</sup>, or TNFR-1 plasmids, and cell viability was measured via the uptake of the vital dye Neutral Red (Sigma) according to the manufacturer's instructions. For the luciferase-based survival assay, a monoclonal population of 293 cells stably transfected with pcDNA3-luciferase was generated by G418 selection (293-Luc). 293-Luc cells were then transfected with control (CAT),  $\Delta$ Np19<sup>ARF</sup>, or TNFR-1 plasmids. For some experiments, cells were transfected 2 days in advance with shRNA plasmids. Cell viability was assessed by measuring luciferase activity (Promega) according to the manufacturer's instructions, using an Anthos Lucy3 Microplate Luminometer. The overall cell survival in the shRNA experiments was determined by dividing the mean luciferase activity (from triplicates) of cells transfected with  $\Delta$ Np19<sup>ARF</sup> by the mean activity of cells transfected with control (CAT) for each knockdown experiment. For trypan blue staining, 293T cells were transfected with control (CAT),  $\Delta$ Np19<sup>ARF</sup>, or TNFR-1 plasmids, and cell death was measured by uptake of trypan blue (Sigma) into cells that had lost membrane integrity.

#### Transmission Electron Microscope

293T cells were transfected with luciferase (control) or  $\Delta$ Np19<sup>ARF</sup> plasmids. Cells were fixed for 1 hr in Karnovsky's fixative (3% paraformaldehyde, 2% glutaraldehyde, 5 mM CaCl<sub>2</sub> in 0.1 M cacodylate buffer [pH 7.4], containing 0.1 M sucrose). Cells were scraped, pelleted, and embedded with agar noble to a final concentration of 1.7% and postfixed with 1% OsO<sub>4</sub>, 0.5% potassium dichromate, and 0.5% potassium hexacyanoferrate in 0.1 M cacodylate buffer. The pellet was stained en bloc with 2% aqueous uranyl acetate followed by ethanol dehydration and embedded in EMbed (EMS). Sections (75 nm) were cut, stained with 2% uranyl acetate in 50% ethanol and lead citrate, and examined using a FEI CM12 EINDHOVEN transmission electron microscope at an accelerating voltage of 120 kV. Digital images were obtained with MegaView3 CCD camera (SIS GMBH).

#### Acknowledgments

We thank N. Mizushima and T. Yoshimori for providing the GFP-LC3 plasmid and anti-ATG5 antibodies. We thank D. Gozuacik for helpful discussions, G. Shohat for help and advice, and A. Gross for reagents and advice. This work was supported by the Israel Science Foundation administered by the Israel Academy of Sciences and Humanities (to A.K.) and by grants from the European Union (LSHB-CT-2004-511983) (to A.K.) and from the Center of Excellence

grant from the Flight Attendant Medical Research Institute (FAMRI) (to A.K. and M.O.). A.K. is the incumbent of the Helena Rubinstein Chair of Cancer Research.

Received: September 14, 2005

Revised: January 13, 2006

Accepted: April 17, 2006

Published: May 18, 2006

#### References

- Bates, S., Phillips, A.C., Clark, P.A., Stott, F., Peters, G., Ludwig, R.L., and Vousden, K.H. (1998). p14ARF links the tumour suppressors RB and p53. *Nature* 395, 124–125.
- Bertwistle, D., Sugimoto, M., and Sherr, C.J. (2004). Physical and functional interactions of the arf tumor suppressor protein with nucleophosmin/b23. *Mol. Cell Biol.* 24, 985–996.
- Boya, P., Gonzalez-Polo, R.A., Casares, N., Perfettini, J.L., Dessen, P., Larochette, N., Metivier, D., Meley, D., Souquere, S., Yoshimori, T., et al. (2005). Inhibition of macroautophagy triggers apoptosis. *Mol. Cell Biol.* 25, 1025–1040.
- Brummelkamp, T.R., Bernards, R., and Agami, R. (2002). A system for stable expression of short interfering RNAs in mammalian cells. *Science* 296, 550–553.
- Cohen, O., Feinstein, E., and Kimchi, A. (1997). DAP-kinase is a Ca<sup>2+</sup>/calmodulin-dependent, cytoskeletal-associated protein kinase, with cell death-inducing functions that depend on its catalytic activity. *EMBO J.* 16, 998–1008.
- Damalas, A., Kahan, S., Shtutman, M., Ben-Ze'ev, A., and Oren, M. (2001). Deregulated beta-catenin induces a p53- and ARF-dependent growth arrest and cooperates with Ras in transformation. *EMBO J.* 20, 4912–4922.
- Elmore, S.P., Qian, T., Grissom, S.F., and Lemasters, J.J. (2001). The mitochondrial permeability transition initiates autophagy in rat hepatocytes. *FASEB J.* 15, 2286–2287.
- Feng, Z., Zhang, H., Levine, A.J., and Jin, S. (2005). The coordinate regulation of the p53 and mTOR pathways in cells. *Proc. Natl. Acad. Sci. USA* 102, 8204–8209.
- Gozuacik, D., and Kimchi, A. (2004). Autophagy as a cell death and tumor suppressor mechanism. *Oncogene* 23, 2891–2906.
- Hemmati, P.G., Gillissen, B., von Haefen, C., Wendt, J., Starck, L., Guner, D., Dorken, B., and Daniel, P.T. (2002). Adenovirus-mediated overexpression of p14(ARF) induces p53 and Bax-independent apoptosis. *Oncogene* 21, 3149–3161.
- Honda, R., and Yasuda, H. (1999). Association of p19(ARF) with Mdm2 inhibits ubiquitin ligase activity of Mdm2 for tumor suppressor p53. *EMBO J.* 18, 22–27.
- Itahana, K., Bhat, K.P., Jin, A., Itahana, Y., Hawke, D., Kobayashi, R., and Zhang, Y. (2003). Tumor suppressor ARF degrades B23, a nucleolar protein involved in ribosome biogenesis and cell proliferation. *Mol. Cell* 12, 1151–1164.
- Jones, R.G., Plas, D.R., Kubek, S., Buzzai, M., Mu, J., Xu, Y., Birnbaum, M.J., and Thompson, C.B. (2005). AMP-activated protein kinase induces a p53-dependent metabolic checkpoint. *Mol. Cell* 18, 283–293.
- Kabeya, Y., Mizushima, N., Ueno, T., Yamamoto, A., Kirisako, T., Noda, T., Kominami, E., Ohsumi, Y., and Yoshimori, T. (2000). LC3, a mammalian homologue of yeast Apg8p, is localized in autophagosome membranes after processing. *EMBO J.* 19, 5720–5728.
- Kuo, M.L., den Besten, W., Bertwistle, D., Rousset, M.F., and Sherr, C.J. (2004). N-terminal polyubiquitination and degradation of the Arf tumor suppressor. *Genes Dev.* 18, 1862–1874.
- Liang, X.H., Jackson, S., Seaman, M., Brown, K., Kempkes, B., Hibshoosh, H., and Levine, B. (1999). Induction of autophagy and inhibition of tumorigenesis by beclin 1. *Nature* 402, 672–676.
- Lohrum, M.A., Ashcroft, M., Kubbutat, M.H., and Vousden, K.H. (2000). Identification of a cryptic nucleolar-localization signal in MDM2. *Nat. Cell Biol.* 2, 179–181.
- Lowe, S.W., and Sherr, C.J. (2003). Tumor suppression by Ink4a-Arf: progress and puzzles. *Curr. Opin. Genet. Dev.* 13, 77–83.

- Matsuoka, M., Kurita, M., Sudo, H., Mizumoto, K., Nishimoto, I., and Ogata, E. (2003). Multiple domains of the mouse p19ARF tumor suppressor are involved in p53-independent apoptosis. *Biochem. Biophys. Res. Commun.* *301*, 1000–1010.
- Midgley, C.A., Desterro, J.M., Saville, M.K., Howard, S., Sparks, A., Hay, R.T., and Lane, D.P. (2000). An N-terminal p14ARF peptide blocks Mdm2-dependent ubiquitination in vitro and can activate p53 in vivo. *Oncogene* *19*, 2312–2323.
- Mihara, M., Erster, S., Zaika, A., Petrenko, O., Chittenden, T., Pantoska, P., and Moll, U.M. (2003). p53 has a direct apoptogenic role at the mitochondria. *Mol. Cell* *11*, 577–590.
- Mills, K.R., Reginato, M., Debnath, J., Queenan, B., and Brugge, J.S. (2004). Tumor necrosis factor-related apoptosis-inducing ligand (TRAIL) is required for induction of autophagy during lumen formation in vitro. *Proc. Natl. Acad. Sci. USA* *101*, 3438–3443.
- Mizushima, N., Yamamoto, A., Hatano, M., Kobayashi, Y., Kabeya, Y., Suzuki, K., Tokuhiya, T., Ohsumi, Y., and Yoshimori, T. (2001). Dissection of autophagosome formation using Apg5-deficient mouse embryonic stem cells. *J. Cell Biol.* *152*, 657–668.
- Nakazawa, Y., Kamijo, T., Koike, K., and Noda, T. (2003). ARF tumor suppressor induces mitochondria-dependent apoptosis by modulation of mitochondrial Bcl-2 family proteins. *J. Biol. Chem.* *278*, 27888–27895.
- Priault, M., Salin, B., Schaeffer, J., Vallette, F.M., di Rago, J.P., and Martinou, J.C. (2005). Impairing the bioenergetic status and the biogenesis of mitochondria triggers mitophagy in yeast. *Cell Death Differ.* *12*, 1613–1621.
- Raveh, T., Droguett, G., Horwitz, M.S., DePinho, R.A., and Kimchi, A. (2001). DAP kinase activates a p19ARF/p53-mediated apoptotic checkpoint to suppress oncogenic transformation. *Nat. Cell Biol.* *3*, 1–7.
- Rodriguez-Enriquez, S., He, L., and Lemasters, J.J. (2004). Role of mitochondrial permeability transition pores in mitochondrial autophagy. *Int. J. Biochem. Cell Biol.* *36*, 2463–2472.
- Shimizu, S., Kanaseki, T., Mizushima, N., Mizuta, T., Arakawa-Kobayashi, S., Thompson, C.B., and Tsujimoto, Y. (2004). Role of Bcl-2 family proteins in a non-apoptotic programmed cell death dependent on autophagy genes. *Nat. Cell Biol.* *6*, 1221–1228.
- Stott, F.J., Bates, S., James, M.C., McConnell, B.B., Starborg, M., Brookes, S., Palmero, I., Ryan, K., Hara, E., Vousden, K.H., and Peters, G. (1998). The alternative product from the human CDKN2A locus, p14(ARF), participates in a regulatory feedback loop with p53 and MDM2. *EMBO J.* *17*, 5001–5014.
- Sugimoto, M., Kuo, M.L., Roussel, M.F., and Sherr, C.J. (2003). Nucleolar Arf tumor suppressor inhibits ribosomal RNA processing. *Mol. Cell* *11*, 415–424.
- Suzuki, H., Kurita, M., Mizumoto, K., Nishimoto, I., Ogata, E., and Matsuoka, M. (2003). p19ARF-induced p53-independent apoptosis largely occurs through BAX. *Biochem. Biophys. Res. Commun.* *312*, 1273–1277.
- Tao, W., and Levine, A.J. (1999). P19(ARF) stabilizes p53 by blocking nucleo-cytoplasmic shuttling of Mdm2. *Proc. Natl. Acad. Sci. USA* *96*, 6937–6941.
- Tsuji, K., Mizumoto, K., Sudo, H., Kouyama, K., Ogata, E., and Matsuoka, M. (2002). p53-independent apoptosis is induced by the p19ARF tumor suppressor. *Biochem. Biophys. Res. Commun.* *295*, 621–629.
- Weber, J.D., Taylor, L.J., Roussel, M.F., Sherr, C.J., and Bar-Sagi, D. (1999). Nucleolar Arf sequesters Mdm2 and activates p53. *Nat. Cell Biol.* *1*, 20–26.
- Weber, J.D., Jeffers, J.R., Rehg, J.E., Randle, D.H., Lozano, G., Roussel, M.F., Sherr, C.J., and Zambetti, G.P. (2000a). p53-independent functions of the p19(ARF) tumor suppressor. *Genes Dev.* *14*, 2358–2365.
- Weber, J.D., Kuo, M.L., Bothner, B., DiGiandomino, E.L., Kriwacki, R.W., Roussel, M.F., and Sherr, C.J. (2000b). Cooperative signals governing ARF-mdm2 interaction and nucleolar localization of the complex. *Mol. Cell Biol.* *20*, 2517–2528.
- Yu, L., Alva, A., Su, H., Dutt, P., Freundt, E., Welsh, S., Baehrecke, E.H., and Lenardo, M.J. (2004). Regulation of an ATG7-beclin 1 program of autophagic cell death by caspase-8. *Science* *304*, 1500–1502.
- Zindy, F., Eischen, C.M., Randle, D.H., Kamijo, T., Cleveland, J.L., Sherr, C.J., and Roussel, M.F. (1998). Myc signaling via the ARF tumor suppressor regulates p53-dependent apoptosis and immortalization. *Genes Dev.* *12*, 2424–2433.